ACS APPLIED MATERIALS & INTERFACES

Research Article

www.acsami.org

Cobalt-Free Nickel Rich Layered Oxide Cathodes for Lithium-Ion Batteries

Yang-Kook Sun,*[,†,⊥] Dong-Ju Lee,[†] Yun Jung Lee,*[,†] Zonghai Chen,[‡] and Seung-Taek Myung*[,§]

[†]Department of Energy Engineering, Hanyang University, Seoul 133-791, Republic of Korea

[‡]Chemical Sciences and Engineering Division, Argonne National Laboratory, 9700 South Cass Avenue, Lemont, Illinois 60439, United States

[§]Department of Nano Engineering, Sejong University, Seoul 143-747, Republic of Korea

[⊥]Chemistry Department, Faculty of Science, King Abdulaziz University, Jeddah, Saudi Arabia

ABSTRACT: We propose a feasibility of Co-free Ni-rich $Li(Ni_{1-x}Mn_x)O_2$ layer compound. $Li(Ni_{1-x}Mn_x)O_2$ $(0.1 \leq x \leq 0.5)$ have been synthesized by a coprecipitation method. Rietveld refinement of X-ray diffraction and microscopic studies reveal dense and spherical secondary particles of highly crystalline phase with low cation mixing over the whole compositions, implying successful optimization of synthetic conditions. Electrochemical test results indicated that the Co-free materials delivered high capacity with excellent capacity retention and reasonable rate capability. In particular, $Li(Ni_{0.9}Mn_{0.1})O_2$, which possesses the lowest cation mixing in the Li layers among samples, exhibited exceptionally high rate capacity (approximately 149 mAh g^{-1} at 10 *C* rate) at 25 °C and high discharge capacity upon cycling under a severe condition, in the voltage range of 2.7−4.5 V at 55 °C. The cation mixing in $Li(Ni_{0.9}Mn_{0.1})O_2$ increased slightly even after the extensive cycling at the elevated temperature, which is ascribed to the structural integrity induced from the optimized synthetic condition using the coprecipitation.

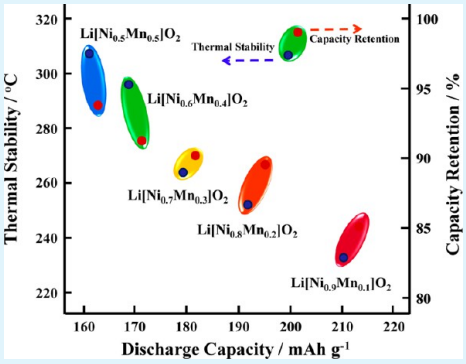

KEYWORDS: *lithium ion battery, cathode, layered oxide, cobalt-free, nickel rich, manganese substitution*

1. INTRODUCTION

Although there have been numerous efforts for the development of alternatives, layered oxides especially based on $LiCoO_2$ still constitute the majority of cathode materials in commercialized lithium-ion batteries (LIBs). To evade the challenges arisen from the scarcity, high cost, and toxicity of the cobalt without compromising capacity,[1−3] cobalt-free layered oxide has been actively searched for. Among the cobalt-free layered oxides, $LiNiO_2$ is one of the most attractive candidates because it shows higher reversible capacity with lower cost than $LiCoO_2$.[4−6] However, it suffers from the intrinsic thermal instability at the charged state and poor cycle life, both of which are related to the chemical and structural instability of tetravalent nickel[2,7] and divalent nickel[8,9] inevitably formed during the high-temperature treatment of $LiNiO_2$. To circumvent the instability problems associated with nickel, researchers have investigated Mn-substitution.[3,9−11] The resulting $Li(Ni_{1-x}Mn_x)O_2$ series have the same α-$NaFeO_2$ layered structure as in the typical layered oxide materials in the nickel-rich regime $(x \leq 0.5)$, however, the structure transforms into spinel with the Mn-rich composition $(x > 0.5)$.[12] Manganese incorporated in $Li(Ni_{1-x}Mn_x)O_2$ exists as tetravalent Mn^{4+} ions[1,11,13] thus $Li(Ni_{1-x}Mn_x)O_2$ can be represented as $Li(Ni^{2+}{}_xNi^{3+}{}_{1-2x}Mn^{4+}{}_x)O_2$. The electrochemically inactive Mn^{4+} ions circumvent the Jahn−Teller distortions related to the presence of Mn^{3+}, playing a crucial role in stabilizing the structures. However, Mn incorporation favors the cationic disorder[12,14,15] between Li^+ and similar sized Ni^{2+} (0.76 Å(Li^+) vs 0.69 Å(Ni^{2+})). The presence of nickel in the lithium layers impedes the Li^+ ion diffusion that is detrimental to high-rate performances[16,17] and induces a decrease of the reversible capacity.[3] Therefore, compositional optimization for capacity, reversibility, and rate performance is a prerequisite for the development of novel cobalt-free layered oxide cathodes.

Although the structural evolution and thermal stability with the Mn-substitution in the cobalt-free nickel-rich $Li(Ni_xMn_{1-x})O_2$ have been examined by a few groups,[8,12,13] reports on the related electrochemical performances have been limited only to a certain composition such as $LiNi_{0.5}Mn_{0.5}O_2$,[11,16,18,19] $LiNi_{2/3}Mn_{1/3}O_2$,[10,20] and $LiNi_{0.9}Mn_{0.1}O_2$[3] by individual groups. Systematic studies on the structural evolution and associated electrochemical properties with controls over compositions have been scarce.[15,21] Moreover, the reported electrochemical performances were below satisfaction probably due to the lack of the process optimization for each composition.

Herein, we report systematic investigation on the cobalt-free nickel rich layered oxides $Li(Ni_{1-x}Mn_x)O_2$ $(0.1 \leq x \leq 0.5)$ with

Received: August 29, 2013
Accepted: October 15, 2013
Published: October 15, 2013

optimized processes for each composition. These materials were synthesized by a coprecipitation method for metal hydroxide precursor preparation followed by a proper thermal treatment with lithium salt. Coprecipitation of hydroxides has been proven a major breakthrough for the fabrication of battery-grade $Li(Ni_{1-x}Mn_x)O_2$ solid solutions through the intimate mixing of various reagents for higher reactivity and homogeniety compared to the conventional simple solid state reactions.[15,18,22] Uniform distribution of Ni and Mn at the atomic scale and a critical factor for the superior material property, could be accomplished by the coprecipitation method. This study explored the impact of composition on the structure−property relationships and demonstrated unprecedentedly high performance of cobalt-free nickel rich layered oxides for stabilized, high-capacity cathodes for LIBs.

2. EXPERIMENTAL SECTION

2.1. Material Synthesis. Cobalt-free nickel-rich oxides $Li(Ni_{1-x}Mn_x)O_2$ ($0.1 \le x \le 0.5$), were synthesized by a coprecipitation process.[22] Stoichiometric amounts of $NiSO_4{\cdot}6H_2O$ and $MnSO_4{\cdot}5H_2O$ were dissolved in deionized water. Then the solution was pumped continuously into the stirred tank reactor (CSTR, capacity 4 L) under a nitrogen atmosphere. At the same time, 2.0 mol dm^{-3} aqueous solution of NaOH and the desired amount of NH_4OH aqueous solution (chelating agent) were separately pumped into the reactor. The concentration, pH, temperature and stirring speed of the reaction mixture were carefully controlled in the CSTR. The coprecipitated precursor powders $(Ni_{1-x}Mn_x)(OH)_2$ ($0.1 \le x \le 0.5$) were filtered, washed, and dried at 110 °C. These double hydroxide precursor compounds were thoroughly mixed with $LiNO_3$ (x = 0.1, 0.2) and $LiOH{\cdot}H_2O$ (x = 0.3, 0.4, 0.5). Finally, $Li(Ni_{1-x}Mn_x)O_2$ ($0.1 \le x \le 0.5$) were formed by thermal treatment at optimal temperature and atmosphere for each composition showing the best electrochemical performance.

2.2. Characterization. The morphology of the powders was examined with Scanning Electron Microscopy (SEM, S-4800, Hitachi). Powder X-ray diffraction (XRD, Rint-2000, Rigaku, Japan) measurements using Cu Kα were employed to identify the crystalline phase of the synthesized materials from 10 to 130 2θ° with step size of 0.03°. Thermal stability was determined in a differential scanning calorimeter (DSC, 200PC, Netzsch).

2.3. Electrochemical Test. The electrochemical performance of the synthesized cathode materials was assessed in a 2032 coin-type cell. The cell consisted of a cathode and a lithium metal anode separated by a porous polypropylene film. The cathode was fabricated with a mixture of prepared layered oxide powder (85 wt %), carbon black (7.5 wt %), and polyvinylidene fluoride (PVDF) (7.5 wt %) in N-methyl-2-pyrrolidone (NMP). The slurry was spread onto the aluminum foil and dried in a vacuum oven at 110 °C. The electrolyte used was 1.2 M $LiPF_6$ in a 3:7 volume mixture of ethylene carbonate (EC) and ethylmethyl carbonate (EMC) (PANAX ETEC Co., Ltd., Korea).

3. RESULTS AND DISCUSSION

In examining the impact of composition on the structure and property in cobalt-free nickel rich layered oxides $Li(Ni_{1-x}Mn_x)O_2$ ($0.1 \le x \le 0.5$), process optimization is critically important since the electrochemical performances vary significantly, even at the same compositions, with the morphologies, crystallinity, particles sizes, surface areas, degree of cation mixing and many other factors determined by the process conditions.[1,10,20,23−27] The impact of coprecipitation conditions on the structure and property of precursor hydroxides has been reported previously.[22,28] Use of the appropriate coprecipitation reactor, oxygen content in the solution and the chelating NH_4OH profoundly influence on the morphology and structure of the resulting hydroxides.[22,28] It has been also proposed that there is an optimum thermal treatment process for each composition of a transition-metal oxide electrode materials.[20] Higher temperature results in better crystallinity[20,23] but higher cation mixing,[20] larger particle size, and lower surface area.[23] Loss of dense, homogeneous, and spherical morphology[20] and higher cation disorder[24] happen above the optimum temperature, leading to poor electrochemical properties. Optimized conditions for each composition investigated in this study are summarized in Table 1. For synthesizing higher Ni content

Table 1. Optimized Synthesis Process Conditions for Ni-Rich $Li(Ni_{1-x}Mn_x)O_2$ ($0.1 \le x \le 0.5$)

sample	hydroxide precursor synthesis condition	final firing condition
$LiNi_{0.9}Mn_{0.1}O_2$	pH 11.7, NH_4OH/metal ratio = 1.0	730 °C/O_2, 15 h (tube)
$LiNi_{0.8}Mn_{0.2}O_2$	pH 11.7, NH_4OH/metal ratio =1.0	750 °C/O_2, 15 h (tube)
$LiNi_{0.7}Mn_{0.3}O_2$	pH 11.7, NH_4OH/metal ratio = 1.0	820 °C/O_2, 15 h (tube)
$LiNi_{0.6}Mn_{0.4}O_2$	pH 11.0, NH_4OH/metal ratio = 0.2	850 °C/air, 15 h (box)
$LiNi_{0.5}Mn_{0.5}O_2$	pH 11.0, NH_4OH/metal ratio = 0.2	920 °C/air, 15 h (box)

$(Ni_{1-x}Mn_x)OH_2$ compounds ($0.1 \le x \le 0.3$), higher pH and a higher amount of NH_4OH were needed to obtain spherical and dense precipitates, otherwise the precipitate showed irregular morphology and low density. However, lower Ni content $(Ni_{1-x}Mn_x)OH_2$ compounds (x = 0.4, 0.5) precipitated continuously to about 10 μm size at lower pH value and lower amount of NH_4OH, otherwise the growth was slow and irregular morphology was obtained. In addition to the above coprecipitation conditions, calcination temperature and atmosphere were also controlled to exhibit the best electrochemical performance of cobalt-free nickel rich layered oxides $Li(Ni_{1-x}Mn_x)O_2$. As Mn content increased from 10 to 50%, optimum temperature increased from 730 to 920 °C. Similar trend was reported on the optimum firing temperature for $LiNi_{0.4}Mn_{0.5}Co_{0.1}O_2$ and $Li(Ni_{0.45}Mn_{0.45}Co_{0.1})O_2$ synthesized by a coprecipitation method.[1] With the increase of Mn content, mixing between Li^+ and Ni^{2+} increases, thus the optimum temperature for the minimum cation disorder for the corresponding composition might increase. Also as Mn content increases, annealing atmosphere changed from pure O_2 to air with reduced oxygen partial pressure to suppress the oxidation of Ni^{2+}. A tube type furnace was used to secure the O_2 atmosphere during calcination of $Li(Ni_{1-x}Mn_x)O_2$ ($x \le 0.3$).

The structural attributes of the synthesized hydroxide precursors and the final layered lithium transition metal oxides at the optimum conditions for each composition were examined by electron microscopes (SEM) and X-ray powder diffraction (XRD). Figure 1 shows the SEM images of synthesized $(Ni_{1-x}Mn_x)(OH)_2$ ($0.1 \le x \le 0.5$) precursors at each composition. The products have regular, homogeneous morphologies of spherical secondary aggregates with average size of ~10 μm for all compositions. In the enlarged view of the spherical particulates (topmost images), dense secondary aggregates are made of smaller primary particles with needle-like in shape. The gross morphologies of the hydroxide precursors maintained in the final layered oxides $Li(Ni_{1-x}Mn_x)O_2$ ($0.1 \le x \le 0.5$) in Figure 2. The uniform spherical morphologies and the average particle sizes of the secondary

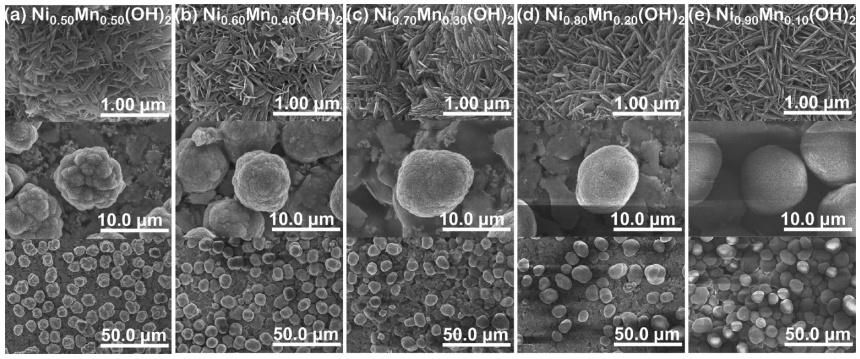

Figure 1. SEM images of the Ni-rich $(Ni_{1-x}Mn_x)(OH)_2$ precursors. (a) $Ni_{0.5}Mn_{0.5}(OH)_2$, (b) $Ni_{0.6}Mn_{0.4}(OH)_2$, (c) $Ni_{0.7}Mn_{0.3}(OH)_2$, (d) $Ni_{0.8}Mn_{0.2}(OH)_2$, and (e) $Ni_{0.9}Mn_{0.1}(OH)_2$.

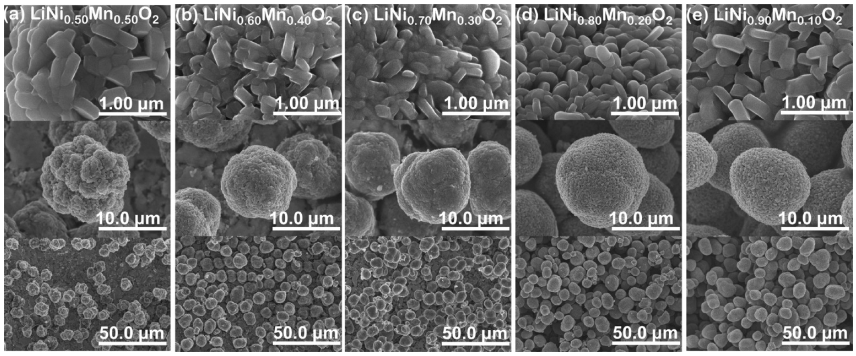

Figure 2. SEM images of the Ni-rich $Li(Ni_{1-x}Mn_x)O_2$. (a) $LiNi_{0.5}Mn_{0.5}O_2$, (b) $LiNi_{0.6}Mn_{0.4}O_2$, (c) $LiNi_{0.7}Mn_{0.3}O_2$, (d) $LiNi_{0.8}Mn_{0.2}O_2$, and (e) $LiNi_{0.9}Mn_{0.1}O_2$.

particles remained almost the same with those of the precursor hydroxides after the heat treatment. The primary needlelike particles, however, were grown to rectangular ones during the high-temperature thermal treatment.

Crystal structure analyses for each composition by XRD are presented in Figure 3. All the samples showed impurity-free single phase of α-$NaFeO_2$ type structure with. The refinement was performed based on the space group $R\bar{3}m$ and chemical

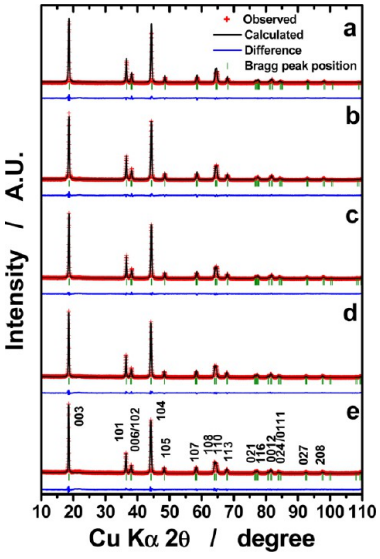

Figure 3. Powder XRD patterns for the Ni-rich $Li(Ni_{1-x}Mn_x)O_2$; x = (a) 0.1, (b) 0.2, (c) 0.3, (d) 0.4, and (e) 0.5.

compositions obtained from atomic absorption spectroscopy (Table 2). Highly crystalline layered structure matched well with the calculated pattern. The cation mixing represented as the amount of Ni^{2+} in Li layer increased with increasing Mn content: For $Li(Ni_{0.9}Mn_{0.1})O_2$, 2.9% of Ni^{2+} was present in the Li layer, but it was increased to 7.3% for $Li(Ni_{0.5}Mn_{0.5})O_2$. Because the total amount of Ni^{2+} increases as Mn content increases in $Li(Ni^{2+}_xNi^{3+}_{1-2x}Mn^{4+}_x)O_2$, Ni^{2+} in Li layer would also increase. The calculated lattice parameters represent the increases in both a and c unit-cell parameters as Mn content increase and Ni content decreases. The "a" cell parameter is the measure of intralayer metal−metal distance and "c" parameter is the sum of MO_6 (M = transition metal) octahedra layer (slab) thickness (slab thickness S) and LiO_6 octahedra layer thickness (interslab thickness I)[3,29] in the lamellar structure of $LiMO_2$. Therefore, the increase in a parameter reflects an increase in the effective ionic radius.[30] Considering the relevant ionic radii[3,24] (Ni^{2+}, 0.69 Å; Ni^{3+}, 0.56 Å; Mn^{4+}, 0.54 Å), the change in the oxidation state of Ni from Ni^{3+} to Ni^{2+}, in particular for the Mn rich composition such as $Li(Ni_{0.5}Mn_{0.5})O_2$, result in the increment of the a-cell parameter. The change in c-cell parameter is the interplay between S and I and closely related with the ionic radii and cation disorder. The presence of larger ions such as Ni^{2+} in the slab contributes to the increase in slab thickness S as in the a-cell parameter; however, cation disorder that displace Ni^{2+} into Li layer (interslab spaces) induces a decrease in interslab thickness I due to the decrease in electrostatic repulsion between the slab.[3,11,30] Hence, the increase in c-cell parameter with Mn content in this study suggests a dominance of the increase in S over the decrease in I.

The electrochemical performances of the optimally synthesized cobalt-free nickel rich layered oxides $Li(Ni_{1-x}Mn_x)O_2$

Table 2. Ratio of Li/Ni/Mn from AAS Analysis, Rietveld Refinement Results for Ni-Rich $Li(Ni_{1-x}Mn_x)O_2$ ($0.1 \le x \le 0.5$)

sample	Li/Ni/Mn composition	Ni^{2+} in Li layer (%)	*a*-axis (Å)	*c*-axis (Å)	Li−O (Å)	M*−O (Å)[a]	R_{wp} (%)	R_p (%)
$LiNi_{0.9}Mn_{0.1}O_2$	1.00/0.89/0.11	2.9(1)	2.8768(2)	14.20932(11)	2.1161(11)	1.9688(15)	11.8	10.0
$LiNi_{0.8}Mn_{0.2}O_2$	1.02/0.79/0.21	5.1(2)	2.8806(2)	14.2329(11)	2.1146(16)	1.9755(14)	10.9	9.79
$LiNi_{0.7}Mn_{0.3}O_2$	1.00/0.70/0.30	5.7(2)	2.8808(2)	14.2452(12)	2.1147(15)	1.9755(13)	9.68	8.79
$LiNi_{0.6}Mn_{0.4}O_2$	1.01/0.60/0.40	6.6(2)	2.8869(2)	14.2853(10)	2.1137(16)	1.9866(14)	10.1	9.58
$LiNi_{0.5}Mn_{0.5}O_2$	0.99/0.51/0.49	7.3(2)	2.8866(2)	14.2965(11)	2.1097(18)	1.9912(16)	11.8	11.6

[a]M* = transition metal (Ni, Mn).

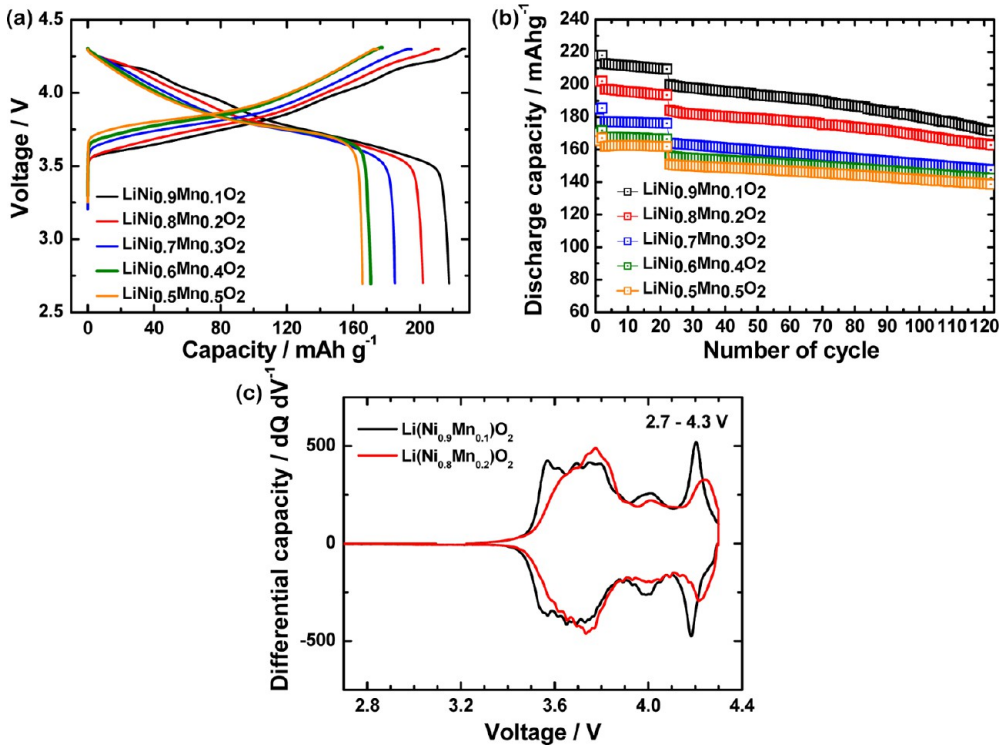

Figure 4. Electrochemical performance of the Ni-rich $Li(Ni_{1-x}Mn_x)O_2$ ($0.1 \le x \le 0.5$) electrodes in a voltage window of 2.7−4.3 V at 30 °C. (a) First charge−discharge curves at a rate of 0.1 C, (b) capacity retention for 120 cycles. 1−20 cycles, 0.2 *C*; and 21−120 cycles: 0.5 *C*. (c) Differential capacity vs voltage curves for $Li(Ni_{0.9}Mn_{0.1})O_2$ and $Li(Ni_{0.8}Mn_{0.2})O_2$ in a.

($0.1 \le x \le 0.5$) were evaluated. Figure 4 shows the comparison of initial charge−discharge curves at a rate of 0.1 C (Figure 4(a)) and the cycling performances (Figure 4b) of the $Li(Ni_{1-x}Mn_x)O_2$ ($0.1 \le x \le 0.5$) in the voltage between 2.5 and 4.3 V at 30 °C. As Mn content increased, the first cycle discharge capacity at 0.1 C decreased from 212.3 mAh g^{-1} ($Li(Ni_{0.9}Mn_{0.1})O_2$) to 163.5 mAh g^{-1} ($Li(Ni_{0.5}Mn_{0.5})O_2$) because Mn^{4+} in these materials are electrochemically inactive. The Coulombic efficiencies at the first cycles were around 95% indicating excellent reversibility for all composition. The cycling test was performed for the first 20 cycles at 0.2 *C*, and the subsequent 100 cycles, then, were carried out at a faster rate of 0.5 *C* in Figure 4b. The capacity retention was improved as Mn content increased due to the chemical and structural stability endowed by Mn. For the first 20 cycles at 0.2 *C*, all compositions showed superior capacity retention; it reached more than 98% at the first 20 cycles (0.2 *C*) for compositions *x* = 0. 3, 0.4, and 0.5 and around 97% for the nickel-rich compositions *x* = 0.1 and 0.2 in $Li(Ni_{1-x}Mn_x)O_2$. In the following 100 cycles at 0.5 C, capacity retention dropped to ~86% (from 98%) for $Li(Ni_{0.9}Mn_{0.1})O_2$, but it decreased less from 99% to 93% for $Li(Ni_{0.5}Mn_{0.5})O_2$ because of the presence of larger amount of stable Mn^{4+}. In Figure 4a, there exists a shoulder in the charge−discharge profile of $Li(Ni_{0.9}Mn_{0.1})O_2$. This shoulder is related to the phase transition of hexagonal to hexagonal (H2 → H3) reported for $LiNiO_2$[31] and nickel-rich layered oxide compounds.[32] Figure 4c shows differential capacity vs voltage profiles ($dQ\ dV^{-1}$) of the two most nickel-rich compositions ($Li(Ni_{0.9}Mn_{0.1})O_2$ and $Li(Ni_{0.8}Mn_{0.2})O_2$) among the compositions tested in this study. Consistent with the previous reports, the redox peak around 4.2 V known as the phase transition of hexagonal to hexagonal (H2 → H3) is prominent for $Li(Ni_{0.9}Mn_{0.1})O_2$and the corresponding peak is not very well-defined for $Li(Ni_{0.8}Mn_{0.2})O_2$ with increasing Mn contents. Although the rapid volume contraction accompanied with the structural changes from H2 to H3 has been reported to affect capacity fading,[31,32] the nickel rich composition $Li(Ni_{0.9}Mn_{0.1})O_2$ showed good cycling stability in Figure 4b. Other noticeable change with increasing Mn content is the increase in polarization in the discharge−charge curves. Because Ni^{2+} ions in the Li layer interrupt the diffusion of Li^+ ions, $Li(Ni_{1-x}Mn_x)O_2$ oxides with increased Mn contents (the higher cation mixing) suffer from kinetic limitations as well as lower electronic conductivity leading larger overpotentials.

Because the chemical and structural instability related to nickel in the layered oxides deteriorate at high temperature and

high potential, the stability of cobalt-free nickel rich layered oxides $Li(Ni_{1-x}Mn_x)O_2$ ($0.1 \le x \le 0.5$) was also explored at higher temperature of 55 °C and higher cutoff potentials of 4.5 V. In Figure 5, the stability at high potential was examined in

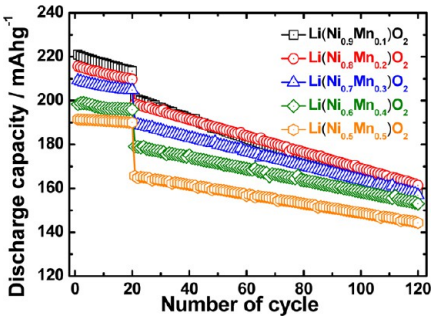

Figure 5. Discharge capacity vs cycle number of the Ni-rich $Li(Ni_{1-x}Mn_x)O_2$ ($0.1 \le x \le 0.5$) electrodes in a voltage window of 2.7−4.5 V at 55 °C. 1−20 cycles, 0.2 *C*; and 21−120 cycles, 0.5 *C*.

the extended voltage window of 2.7−4.5 V at 55 °C. The initial capacities appeared increased due to further deintercalation of Li^+ ions with the higher charging cutoff voltage of 4.5 V. The increase in capacity was more prominent with increasing Mn content due to increased electronic conductivity of Mn-rich materials at the elevated temperature. The capacity retention became worse compared to those in Figure 4 where the voltage cutoff is 4.3 V at 30 °C and the degradation progressed faster as nickel content increased, presumably ascribing to the structural instability of Ni-rich compound. The initial discharge capacities at 0.2 C increased especially for $Li(Ni_{0.5}Mn_{0.5})O_2$ to 191.4 mAh g^{-1}. The capacity retention reached more than 99% at 0.2 *C* and 86% at 0.5 *C*. Interestingly, it is notable that the capacity retention was still good as high as ~78.5% for $LiNi_{0.9}Mn_{0.1}O_2$ during 100 cycles at 0.5 *C*. This result suggests that 10% incorporation of Mn is substantially sufficient to provide cycling stability for the cobalt-free nickel rich layered oxides under this severe condition at the high temperature and high voltage cutoff.

Rate capability of $Li(Ni_{1-x}Mn_x)O_2$ ($0.1 \le x \le 0.5$) cathodes was systematically evaluated from 0.1 to 10 *C* in Figure 6. The rate capabilities of higher Ni content oxides were superior to the ones with increasing Mn content, consistent with the trends reported above in the capacity ratio of 0.5 *C*/0.1 *C*. Again, kinetic hindrance from Ni^{2+} ions in Li layer with increasing Mn content is the reason for the inferior rate performance with

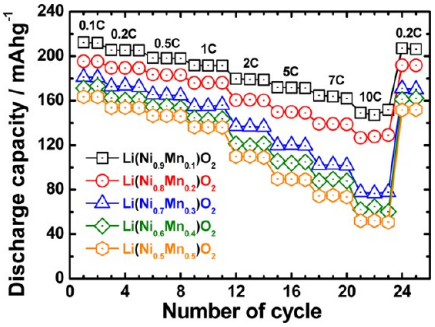

Figure 6. Rate capability of the Ni-rich $Li(Ni_{1-x}Mn_x)O_2$ ($0.1 \le x \le 0.5$) electrodes in a voltage window of 2.7−4.3 V. Electrodes were charged at 0.2 *C* and discharged at the corresponding rates.

increasing Mn content. The discharge capacity of $Li(Ni_{0.9}Mn_{0.1})O_2$ cathodes at 10 C was 160 mAh g^{-1} that corresponds to 76% of the capacity at 0.1 *C* (210 mAh g^{-1}) while the capacity of $Li(Ni_{0.5}Mn_{0.5})O_2$ at 10 C is only 31% (50 mAh g^{-1}) of the value at 0.1 *C* (160 mAh g^{-1}). All of the tested layered oxides $Li(Ni_{1-x}Mn_x)O_2$ ($0.1 \le x \le 0.5$) restored their initial capacities when the test rate returned to the slow rate of 0.1 *C* after cycled from 0.1 to 10 *C*, implying that the high current at fast rates did not damage the structure of the nickel-rich layered oxides.

These results are superior to those reported previously for Co-free Ni-rich $Li(Ni_{1-x}Mn_x)O_2$ cathodes. Especially, $Li(Ni_{0.9}Mn_{0.1})O_2$ showed poor performance in a literature with reversible capacity of only 125 mAh g^{-1} at 0.05 *C* rate in the voltage window of 3−4.15 V.[3] $Li(Ni_{2/3}Mn_{1/3})O_2$ delivered 160−170 mAh g^{-1} at voltage cutoff of 4.5 V, but capacity fading was observed after 50 cycles.[10] Only limited literatures have reported performances comparable to our current results, but only for selected compositions. Discharge capacity of ~200 mAh g^{-1} was delivered in the voltage window of 2.5−4.5 V for $Li(Ni_{0.5}Mn_{0.5})O_2$,[33] but the test lasted only for 30 cycles. $Li(Ni_{2/3}Mn_{1/3})O_2$ showed capacities more than 190 mAh g^{-1} when charged to 4.6 V.[20] However, issues related to restricted cycle life at elevated temperature have not been addressed in their report.

Those extensively cycled electrodes were analyzed by Rietveld refinement (Figure 7). Conducting agent, graphite,

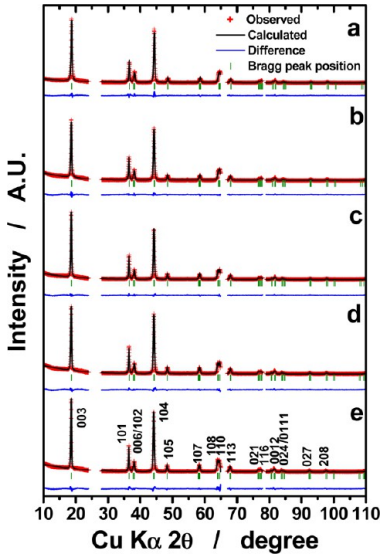

Figure 7. Powder XRD patterns for extensively cycled the Ni-rich $Li(Ni_{1-x}Mn_x)O_2$ electrodes; x = (a) 0.1, (b) 0.2, (c) 0.3, (d) 0.4, and(e) 0.5.

and Al current collector were excluded for the analysis. It is surprising that all the electrodes maintained the original layer structure even after the extensive cycling tests. Because of the poor structural stability, Ni-rich electrode materials usually experienced significant structural disorder after prolonged cycling.[2,18,34] Interestingly, the present $LiNi_{0.9}Mn_{0.1}O_2$ material did not exhibit serious structural change as shown in Tables 2 and 3. A slight increment (3.8%) of cation mixing is observed in the Li layer after the cycling, 6.7% occupation of Ni^{2+} in the Li layer, which is the lowest value among samples. This tendency shows low cation mixing in the Li layer even after extensive

Table 3. Rietveld refinement Results for Ni-Rich $Li(Ni_{1-x}Mn_x)O_2$ (x = 0.1, 0.2, 0.3, 0.4, and 0.5) Electrodes after Extensive Cycling Shown in Figure 5

sample	Ni^{2+} in Li layer (%)	a-axis (Å)	c-axis (Å)	Li−O (Å)	M*−O (Å)[a]	R_{wp} (%)	R_p (%)
$LiNi_{0.9}Mn_{0.1}O_2$	6.7(2)	2.8791(1)	14.2275(8)	2.1105(21)	1.9685(18)	11.8	11.3
$LiNi_{0.8}Mn_{0.2}O_2$	7.7(2)	2.8823(1)	14.2507(8)	2.1112(18)	1.9816(16)	10.2	9.94
$LiNi_{0.7}Mn_{0.3}O_2$	7.1(2)	2.8825(1)	14.2787(7)	2.1146(17)	1.9804(15)	9.65	9.21
$LiNi_{0.6}Mn_{0.4}O_2$	8.5(2)	2.8885(1)	14.2967(7)	2.1044(17)	1.9920(16)	10.7	10.6
$LiNi_{0.5}Mn_{0.5}O_2$	9.0(3)	2.8892(1)	14.3048(8)	2.1065(21)	1.9942(18)	13.3	12.5

[a]M* = transition metal (Ni, Mn).

cycling for the $LiNi_{0.9}Mn_{0.1}O_2$ composition. As a result, it is evident that the superior cyclability and rate capability is ascribed to the structural integrity of the present $Li-Ni_{0.9}Mn_{0.1}O_2$. The difference compared to the conventional Ni-rich materials[35−38] is the coprecipitation synthesis attaining spherical and dense secondary particle morphology. This morphological advantage has beneficial effect in reducing side reaction with HF-generating electrolyte during cycling. Although the Mn content increased, the variation in the cation mixing did not significantly vary from the present $Li-Ni_{0.9}Mn_{0.1}O_2$, showing increment of 1.7−2.2% for the other compositions after the cycling. The slight increase in the a-axis parameter is due to the presence larger Ni^{2+} in the Li layer formed during cycling. We believe that the structural integrity endowed by the optimized synthesis is the reason for the excellent electrode performance of the $Li(Ni_{0.9}Mn_{0.1})O_2$ ever reported, to the best of our knowledge. Another factor considered is the absence of the Co element in the compound. Addition of Co ingredient seems to be good because the presence of Co improves electric conductivity, which affects rate performance and lowered cation mixing by forming a solid solution with $LiCoO_2$. By contrast, Co containing layered material would be exposed in an inappropriate situation through Co dissolution at deeply charged state, which simultaneously structural instability.[18,39−43] Therefore, we conclude that Co-free composition is more desirable in terms of structural stability and electrode performance upon cycling.

The variation in thermal stability with composition was investigated in the DSC measurement of the charged electrodes in Figure 8. The cells using nickel-rich layered oxides $Li(Ni_{1-x}Mn_x)O_2$ ($0.1 \le x \le 0.5$) were charged to 4.3 V at a rate of 0.2 C. As expected the thermal property was greatly dependent on the amount of present Mn in the compound. Interesting point is that the lowest Mn content, $Li(Ni_{0.9}Mn_{0.1})-O_2$ had relatively high main exothermic temperature of 230.4 °C and relatively low heat evolution of 901.4 J g^{-1} compared to other delithiated Ni-rich compounds. As we reported early, the main exothermic reaction is deeply related with the formation of cubic spinel phase as a result of oxygen release from the host structure.[41,44] Hence, the delayed exothermic reaction implies that the spinel phase could be formed at elevated temperature, which would be attributed to the improved structural integrity as evidenced from the Rietveld refinement data (Figures 3 and 7). Therefore, we conclude that optimization of synthetic condition is significantly important to improve capacity, its retention, rate capability and thermal properties.

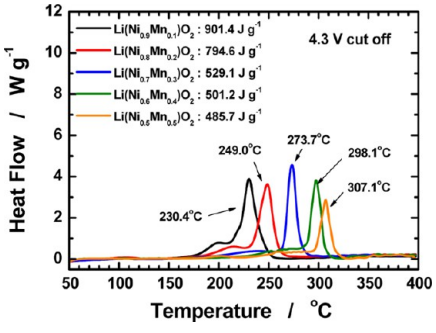

Figure 8. DSC profiles of the Ni-rich $Li(Ni_{1-x}Mn_x)O_2$ (x = 0.1, 0.2, 0.3, 0.4, and 0.5) electrodes with a scan rate 5 °C min^{-1}. The cells were charged to 4.3 V at the rate of 0.2 C.

4. CONCLUSIONS

So far, though we believed the poor electrode performance of cobalt-free nickel rich layered oxides $Li(Ni_{1-x}Mn_x)O_2$ ($0.1 \le x \le 0.5$), this paper revisited the nickel-rich compounds to improve the electrochemical performance due to their high capacity. Among the Ni-rich compounds, our synthetic optimization of the $Li(Ni_{0.9}Mn_{0.1})O_2$ material endorses the potential possibility of the electrode enabling high capacity retention and high rate capability as well, compared to any existing Ni-rich electrodes in the same chemical composition reported ever. Rietveld refinement results of XRD data described lower cation mixing in the as-synthetized state (2.9%) and slightly increment even after the extensive cycling at 55 °C (6.7%), which is greatly related to the high capacity retention, fast rate properties, and thermal properties. Through realization of the synthetic optimization, we propose that the present $Li(Ni_{0.9}Mn_{0.1})O_2$ material can be substantially available as cathode materials for high capacity rechargeable lithium batteries.

AUTHOR INFORMATION

Corresponding Authors

*E-mail: yksun@hanyang.ac.kr. Tel: 82 2 2220 0524. Fax: 82 2 2282 7329.

*E-mail: yjlee94@hanyang.ac.kr. Tel: 82 2 2220 2411. Fax: 82 2 2282 7329;

*E-mail: smyung@sejong.ac.kr. Tel: 82 2 3408 3454. Fax: 82 2 3408 4342.

Notes

The authors declare no competing financial interest.

ACKNOWLEDGMENTS

This work was supported by the National Research Foundation of Korea (NRF) grant funded by the Korea government (MEST) (2009-0092780) and the Global Frontier R&D Program (2013-073298) on Center for Hybrid Interface Materials (HIM) funded by the Ministry of Science, ICT & Future Planning.

REFERENCES

(1) Xiao, J.; Chernova, N. A.; Whittingham, M. S. *Chem. Mater.* **2010**, *22*, 1180−1185.
(2) Sun, Y. K.; Chen, Z. H.; Noh, H. J.; Lee, D. J.; Jung, H. G.; Ren, Y.; Wang, S.; Yoon, C. S.; Myung, S. T.; Amine, K. *Nat. Mater.* **2012**, *11*, 942−947.
(3) Guilmard, M.; Croguennec, L.; Delmas, C. *J. Electrochem. Soc.* **2003**, *150*, A1287−A1293.
(4) Dahn, J. R.; Vonsacken, U.; Juzkow, M. W.; Aljanaby, H. *J. Electrochem. Soc.* **1991**, *138*, 2207−2211.
(5) Broussely, M.; Perton, F.; Labat, J.; Staniewicz, R. J.; Romero, A. *J. Power Sources* **1993**, *43*, 209−216.
(6) Ohzuku, T.; Ueda, A. *Solid State Ioics.* **1994**, *69*, 201−211.
(7) Abraham, D. P.; Twesten, R. D.; Balasubramanian, M.; Petrov, I.; McBreen, J.; Amine, K. *Electrochem. Commun.* **2002**, *4*, 620−625.
(8) Spahr, M. E.; Novak, P.; Schnyder, B.; Haas, O.; Nesper, R. *J. Electrochem. Soc.* **1998**, *145*, 1113−1121.
(9) Hwang, B. J.; Tsai, Y. W.; Chen, C. H.; Santhanam, R. *J. Mater. Chem.* **2003**, *13*, 1962−1968.
(10) Reddy, M. V.; Rao, G. V. S.; Chowdari, B. V. R. *J. Power Sources* **2006**, *160*, 1369−1374.
(11) Yabuuchi, N.; Kim, Y.-T.; Li, H. H.; Shao-Horn, Y. *Chem. Mater.* **2008**, *20*, 4936−4951.
(12) Rossen, E.; Jones, C. D. W.; Dahn, J. R. *Solid State Ioics.* **1992**, *57*, 311−318.
(13) Kobayashi, H.; Sakaebe, H.; Kageyama, H.; Tatsumi, K.; Arachi, Y.; Kamiyama, T. *J. Mater. Chem.* **2003**, *13*, 590−595.
(14) Hirano, A.; Kanno, R.; Kawamoto, Y.; Nitta, Y.; Okamura, K.; Kamiyama, T.; Izumi, F. *J. Solid State Chem.* **1997**, *134*, 1−4.
(15) Caurant, D.; Baffier, N.; Bianchi, V.; Gregoire, G.; Bach, S. *J. Mater. Chem.* **1996**, *6*, 1149−1155.
(16) Ohzuku, T.; Makimura, Y. *Chem. Lett.* **2001**, 744−745.
(17) Yabuuchi, N.; Ohzuku, T. *J. Power Sources* **2003**, *119*, 171−174.
(18) Sun, Y. K.; Myung, S. T.; Park, B. C.; Yashiro, H. *J. Electrochem. Soc.* **2008**, *155*, A705−A710.
(19) Koyama, Y.; Makimura, Y.; Tanaka, I.; Adachi, H.; Ohzuku, T. *J. Electrochem. Soc.* **2004**, *151*, A1499−A1506.
(20) Zhou, F.; Zhao, X.; Smith, A. J.; Dahn, J. R. *J. Electrochem. Soc.* **2010**, *157*, A399−A406.
(21) Arai, H.; Okada, S.; Sakurai, Y.; Yamaki, J. *J. Electrochem. Soc.* **1997**, *144*, 3117−3125.
(22) Lee, M. H.; Kang, Y. J.; Myung, S. T.; Sun, Y. K. *Electrochim. Acta* **2004**, *50*, 939−948.
(23) Xiao, J.; Chernova, N. A.; Whittingham, M. S. *Chem. Mater.* **2008**, *20*, 7454−7464.
(24) Ngala, J. K.; Chernova, N. A.; Ma, M. M.; Mamak, M.; Zavalij, P. Y.; Whittingham, M. S. *J. Mater. Chem.* **2004**, *14*, 214−220.
(25) Lee, K. S.; Myung, S. T.; Moon, J. S. M.; Sun, Y. K. *Electrochim. Acta* **2008**, *53*, 6033−6037.
(26) Lee, K. S.; Myung, S. T.; Prakash, J.; Yashiro, H.; Sun, Y. K. *Electrochim. Acta* **2008**, *53*, 3065−3074.
(27) Rao, C. V.; Reddy, A. L. M.; Ishikawa, Y.; Ajayan, P. M. *ACS Appl. Mater. Interfaces* **2011**, *3*, 2966−2972.
(28) Zhou, F.; Zhao, X.; van Bommel, A.; Rowe, A. W.; Dahn, J. R. *Chem. Mater.* **2010**, *22*, 1015−1021.
(29) Mahmoud, A.; Yoshita, M.; Saadoune, I.; Broetz, J.; Fujimoto, K.; Ito, S. *Mater. Res. Bull.* **2012**, *47*, 1936−1941.
(30) Sekizawa, O.; Hasegawa, T.; Kitamura, N.; Idemoto, Y. *J. Power Sources* **2011**, *196*, 6651−6656.
(31) Li, W.; Reimers, J. N.; Dahn, J. R. *Solid State Ionics* **1993**, *67*, 123−130.
(32) Noh, H. J.; Youn, S.; Yoon, C. S.; Sun, Y. K. *J. Power Sources* **2013**, *233*, 121−130.
(33) Makimura, Y.; Ohzuku, T. *J. Power Sources* **2003**, *119*, 156−160.
(34) Sun, Y. K.; Myung, S. T.; Park, B. C.; Prakash, J.; Belharouak, I.; Amine, K. *Nat. Mater.* **2009**, *8*, 320−324.
(35) Ju, S. H.; Jang, H. C.; Kang, Y. C. *Electrochim. Acta* **2007**, *52*, 7286−7292.
(36) Ju, S. H.; Kang, Y. C. *J. Power Sources* **2008**, *178*, 387−392.
(37) Hwang, I.; Lee, C. W.; Kim, J. C.; Yoon, S. *Mater. Res. Bull.* **2012**, *47*, 73−78.
(38) Sun, Y. K.; Myung, S. T.; Kim, M. H.; Prakash, J.; Amine, K. *J. Am. Chem. Soc.* **2005**, *127*, 13411−13418.
(39) Myung, S. T.; Kumagai, N.; Komaba, S.; Chung, H. T. *Solid State Ionics* **2001**, *139*, 47−56.
(40) Amatucci, G. G.; Tarascon, J. M.; Klein, L. C. *Solid State Ionics* **1996**, *83*, 167−173.
(41) Myung, S. T.; Ogata, A.; Lee, K. S.; Komaba, S.; Sun, Y. K.; Yashiro, H. *J. Electrochem. Soc.* **2008**, *155*, A374−A383.
(42) Lee, K. S.; Myung, S. T.; Amine, K.; Yashiro, H.; Sun, Y. K. *J. Electrochem. Soc.* **2007**, *154*, A971−A977.
(43) Sun, Y. K.; Myung, S. T.; Bang, H. J.; Park, B. C.; Park, S. J.; Sung, N. Y. *J. Electrochem. Soc.* **2007**, *154*, A937−A942.
(44) Myung, S. T.; Lee, K. S.; Yoon, C. S.; Sun, Y. K.; Amine, K.; Yashiro, H. *J. Phys. Chem. C* **2010**, *114*, 4710−4718.